

Transverse and longitudinal confinement of photonic nanojets by compound dielectric microspheres

Alexis Devilez, Jérôme Wenger, Brian Stout, Nicolas Bonod*
Institut Fresnel, Aix-Marseille university, CNRS, 13397 Marseille, France

*corresponding author : nicolas.bonod@fresnel.fr

ABSTRACT

We discuss the compound set of two dielectric microspheres to confine light in a three dimensional region of dimensions on the order of the wavelength when the spheres are illuminated by a plane wave. This simple configuration enables the reduction of the longitudinal dimension of so called photonic jets, together with a strong focusing effect. The beam shaped in that way is suitable for applications requiring high longitudinal resolutions and/or strong peak intensities.

Keywords: Micro-optical devices; Mie theory; Electromagnetic optics; scattering, particles;

1. INTRODUCTION

Strong concentration of light in region of subwavelength dimension is widely investigated to localize and enhance light/matter interactions in various applications such as sensing, ultramicroscopy, spectroscopy or optical data storage. Metallic structures such as gratings, pinholes, tips or nanoparticles [1-4], which take advantage of electromagnetic resonances such as plasmon modes, or resonant dielectric structures such as gratings or photonic crystal cavities [5-7] are commonly used because they offer strong confinements of the electromagnetic field. However, these performances come at the expense of complicated structures and challenging nanofabrication process.

In the search for simple dielectric structures to concentrate light at the nanoscale, dielectric spheres of micrometer dimensions have been recently investigated [8-14]. When the microsphere is illuminated by a plane wave, the so-called “photonic nanojet” beam that emerges from the sphere has subwavelength transverse dimensions and low divergence, which makes it fruitful for applications in dry laser cleaning [15, 16], nanopatterning [17-19], Raman spectroscopy [20, 21] and optical data storage [22]. However, the classical photonic nanojet performs no better than the focusing obtained from a classical microscope objective with a high numerical aperture. Its large dimension along the optical axis makes the photonic nanojet unsuitable for applications requiring high transverse and longitudinal resolutions. Recently, it has been shown that a single microsphere illuminated by a tightly focused Gaussian beam can outperform classical microscope systems and significantly enhance the fluorescence emission from a single molecule [23]. In that case, strong confinement of light, on the order of $0.6 \times (\lambda/n)^3$, with a non-resonant dielectric structure was clearly demonstrated [24].

We assume that this phenomenon can be applied to any focused beam and propose to set a microsphere in a photonic jet beam in order to reduce its longitudinal extent. In this paper, employing rigorous Lorentz-Mie theory [25], we demonstrate that a plane wave can be confined in a region on the order of $(\lambda/n)^3$ using a compound lens of two dielectric microspheres. To support our work, photonic jets are studied, in a first section, in both direct and reciprocal spaces and compared with classical Gaussian beams.

2. PHOTONIC NANOJETS CHARACTERISATION

Diffraction of light on a micrometric sized sphere is a well established electromagnetic problem solved a century ago by Mie. He predicted that a dielectric microsphere illuminated by a plane wave mostly scatters light in the forward direction. Until recently, this effect was considered as a trivial focusing effect. In 2004, Chen et al. have shown that the beam that emerges has features of particular interest such as a subwavelength transversal dimension combined to micrometric longitudinal extent [8]. In the need to understand further the features of photonic jets, a study in both direct space and reciprocal space has to be carried out.

2.1 Direct space feature of photonic nanojets

Figure 1 presents the electric field intensity map when a single $6\mu\text{m}$ diameter sphere of refractive index (a) $n_s = 2$ and (b) $n_s = 1.6$ is illuminated by a plane wave. The intensity pattern shows a typical so called photonic nanojet beam which has a narrow transversal extent of around 400 nm (at $1/e^2$) but a large longitudinal extent of (a) $1.8\mu\text{m}$ and (b) $6\mu\text{m}$. The longitudinal extension of the photonic beam strongly depends on the contrast of refractive index $\rho = n_s/n_0$ between the microsphere and the host medium. The dimension of photonic jets along the optical axis is particularly large for low index contrasts. For applications such as particles sensing or nanopatterning, requiring high transverse and longitudinal resolution in water-based solution or polymeric media, photonic jets are unsuitable. In addition, the microsphere focuses light far from the sphere. It results that multiple lobes of intense field are present between the sphere and the main beam which may spoil expected results.

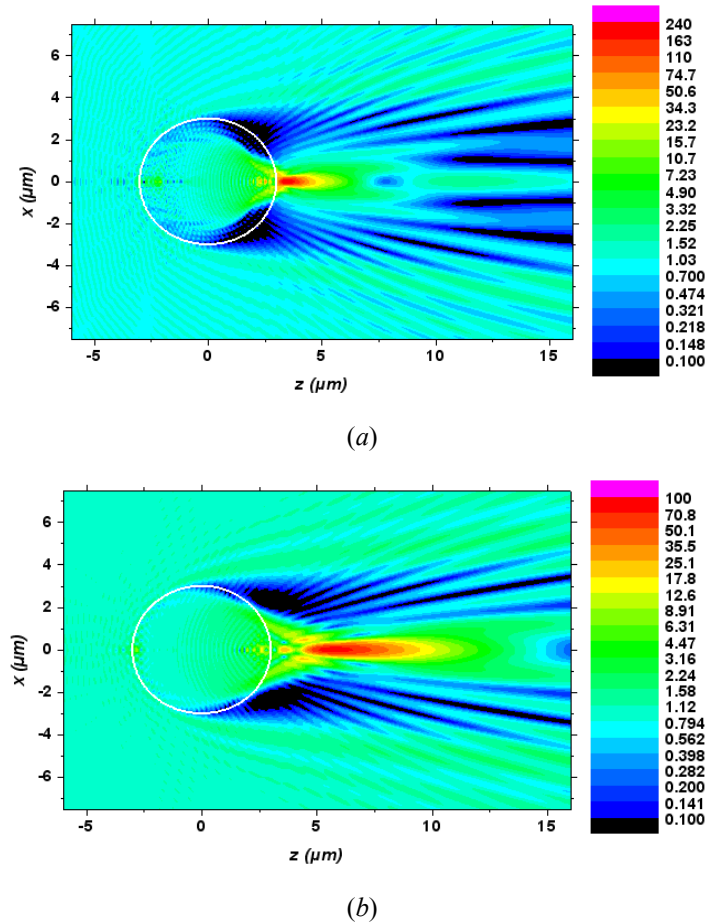


Fig. 1. Intensity colored map in logarithmic scale of a $6\mu\text{m}$ diameter sphere illuminated by a plane wave at $\lambda = 633\text{ nm}$. In both cases the sphere is surrounded by water ($n_0 = 1.33$). The refractive index of the sphere is (a) $n_s = 2$ and (b) $n_s = 1.6$.

To characterize photonic jets, the intensity enhancement of the electromagnetic field has been displayed on two axes of interest: the propagation axis z and a transverse axis x at $z = z(I_{max})$. An example is presented in Fig. 2, for a diameter $D = 3\mu\text{m}$ and $\rho = 1.2$. It has been found that the intensity enhancement along the propagation axis z , displayed in Fig. 2(a), can be fitted in its decreasing part by a Lorentzian distribution. At the same time, the transversal intensity enhancement, displayed in Fig. 2(b) can be predominantly fitted by a Gaussian distribution. As the longitudinal intensity distribution of figure 2(a) is not symmetric with respect to the I_{max} position, we define two longitudinal waists for the incident photonic jet beam, w_{z-} and w_{z+} , which are respectively the waist (I_{max}/e^2) before and after the I_{max} position.

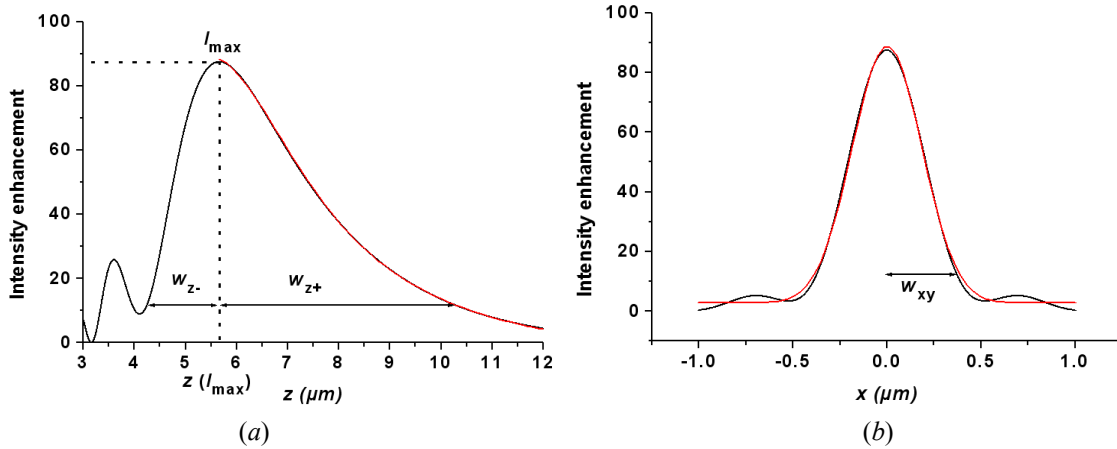


Fig. 2. Intensity enhancement distribution for a 6 μm diameter sphere illuminated by a plane wave at $\lambda_v = 633$ nm with an index contrast of $\rho = 1.2$, $\lambda_0 = \lambda_v/n_0 = 476$ nm (a) along the propagation axis (z) (in black), and its Lorentzian fit (in red), $w_{z-} = 1400$ nm and $w_{z+} = 4590$ nm (b) along a transverse axis (x) for $z(I_{\max}) = 5.66$ μm (in black), and its Gaussian fit (in red), $w_{xy} = 375$ nm $= 0.78 \times \lambda_0$.

Despite these similarities with Gaussian beam distributions, it can be argued that photonic jets are more accurately described in terms of Bessel beams of variable cross sections [12]. However, Gaussian beams are generated by classical optical devices, and commonly encountered in experiments. This comparison can lead to a practical understanding of photonic jet properties and of the phenomena described later in this paper. As could be expected, photonic jets nevertheless differ from Gaussian beams, especially with respect to the way in which they propagate. The study of the spatial frequencies involved in the photonic jets field distribution will be particularly useful in distinguishing photonic jets from Gaussian beams.

2.2 Study in reciprocal space: role of high angular components

A rigorous angular spectral analysis of the scattered field is performed here by expanding the partial waves on plane waves [14-16] to calculate the EM field. In Lorentz-Mie theory, the scattered field is expanded on a set of Vector Spherical Wave Functions (VSWFs), commonly denoted $\mathbf{M}_{n,m}$ and $\mathbf{N}_{n,m}$ [25]:

$$\mathbf{E}_{\text{scat}}(r, \theta, \phi) = E_0 \sum_{n=1}^{\infty} \sum_{m=-n}^n f_{n,m}^{(h)} \mathbf{M}_{n,m}(k_0 r, \theta, \phi) + f_{n,m}^{(e)} \mathbf{N}_{n,m}(k_0 r, \theta, \phi) \quad (1)$$

where $f_{n,m}$ are the Mie coefficients for scattered field and $k_0 = 2\pi N_0/\lambda_v$ is the propagation wave vector in the host medium. The details of our notations are given in Ref. [14]. Expressing the transverse wavevector $\vec{\mathbf{K}}$ as:

$$\vec{\mathbf{K}} = K \cos \phi_k \hat{\mathbf{x}} + K \sin \phi_k \hat{\mathbf{y}}, \quad (2)$$

one can write a spectral decomposition of the outgoing VSWFs in the form:

$$\begin{aligned} \mathbf{M}_{n,m}(k_0 r_{//}, \phi, z) &= \int_{K=0}^{\infty} \int_{\phi=0}^{2\pi} \mathbf{X}_{n,m}(\theta_k, \phi_k) \frac{e^{i(\vec{\mathbf{K}} \cdot \vec{r}_{//} + k_z |z|)}}{k_z} K dK d\phi_k \\ \mathbf{N}_{n,m}(k_0 r_{//}, \phi, z) &= \int_{K=0}^{\infty} \int_{\phi=0}^{2\pi} \mathbf{Z}_{n,m}(\theta_k, \phi_k) \frac{e^{i(\vec{\mathbf{K}} \cdot \vec{r}_{//} + k_z |z|)}}{k_z} K dK d\phi_k \end{aligned} \quad (3)$$

where $(r_{//}, \phi, z)$ are cylindrical coordinates and $k_z = \sqrt{k_0^2 - K^2}$. One can observe that the VSWFs can be interpreted as the angular spectrum of the vector spherical harmonics in the cylindrical wave representation. Spectral decompositions were here and henceforth restricted to the scattered field since they are unsuitable for describing incident plane waves (which are represented by a Dirac distributions at $K = 0$).

To proceed further, we adopt the simplifying case of a sphere illuminated by a circularly right-polarized incident plane wave so that the field is entirely described by VSWFs with $m = 1$ (arbitrary polarization can of course be obtained by superpositions with circularly left polarized waves, $m = -1$). Using the Cartesian vector spherical harmonics, the scattered field can be written as:

$$\mathbf{E}_{\text{scat}}(r_{//}, \phi, z) = E_0 \int_0^\infty \frac{K}{k_0} d \frac{K}{k_0} \begin{bmatrix} A\left(\frac{K}{k_0}, \phi, z\right) J_0(Kr_{//}) \frac{\{\hat{\mathbf{x}} + i\hat{\mathbf{y}}\}}{\sqrt{2}} \\ B\left(\frac{K}{k_0}, \phi, z\right) J_1(Kr_{//}) \hat{\mathbf{z}} \\ C\left(\frac{K}{k_0}, \phi, z\right) J_2(Kr_{//}) \frac{\{\hat{\mathbf{x}} - i\hat{\mathbf{y}}\}}{\sqrt{2}} \end{bmatrix} \quad \text{with} \quad \begin{aligned} A &= \sum_{n=0}^{\infty} f_n^{(h)} A_n^{(h)} + f_n^{(e)} A_n^{(e)} \\ B &= \sum_{n=0}^{\infty} f_n^{(h)} B_n^{(h)} + f_n^{(e)} B_n^{(e)} \\ C &= \sum_{n=0}^{\infty} f_n^{(h)} C_n^{(h)} + f_n^{(e)} C_n^{(e)} \end{aligned} \quad (4)$$

where details and full expressions are relegated to Appendix B of Ref. [14]. This expansion provides the angular spectrum of plane waves representation of the field via three different coefficient functions, A , B , and C . We focus our attention on the amplitude of the preponderant spectral component $|A|$.

The amplitude of A is presented in Fig. 3 as a function of the normalized radial spatial frequencies K/k_0 for a sphere of radius $R = 3 \mu\text{m}$ at the position $\phi = 0$, $z = 3.001 \mu\text{m}$. $|A|$ is normalized to 1 at $K = 0$, and plotted for two different index contrasts $\rho = 1.2$ in Fig. 3(a) and $\rho = 1.5$ in Fig. 3(b). The radial spectrum has the following features: a generally decreasing and oscillating features in the region $0 < K/k_0 < 1$ corresponding to propagative fields, a singularity originating from the homogeneous medium Green function at $K/k_0 = 1$ and a monotonically decreasing behaviour when $K > k_0$ for evanescent field contributions.

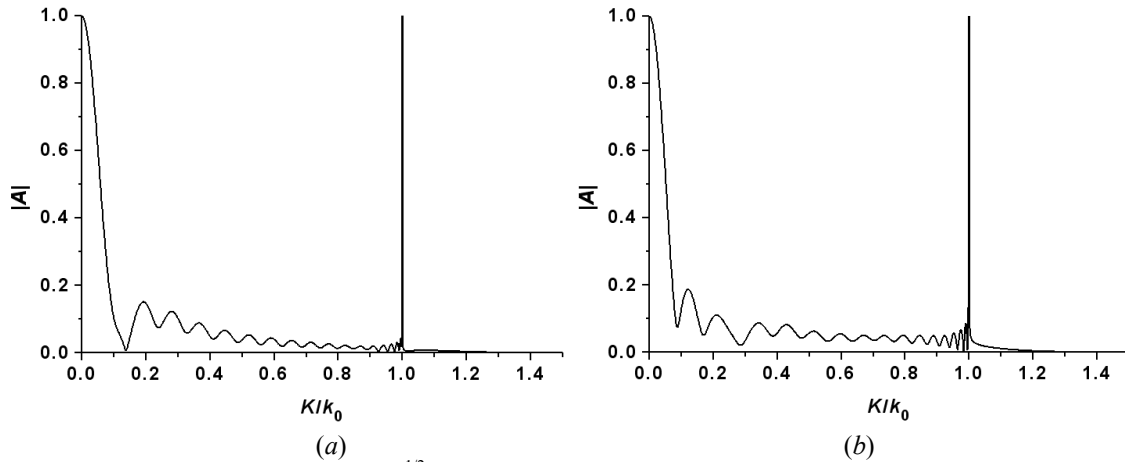


Fig. 3. Total spectral amplitude $|A| = (AA^*)^{1/2}$ as a function of normalized spatial frequencies K/k_0 at $z = 3.001 \mu\text{m}$, for a sphere of radius $R = 3 \mu\text{m}$, and index contrasts (a) $\rho = 1.2$ and (b) $\rho = 1.5$, illuminated by a plane wave at $\lambda_v = 633 \text{ nm}$.

The propagative frequency decomposition can be separated in two regions of interest. From the zero-frequency to the first minimum, the spectral distribution can be described by a narrow Gaussian-type distribution. The secondary maxima and minima which can be observed in the higher spatial propagative frequencies enrich the jet spectrum. These secondary maxima result in photonic jets having features that differ from Gaussian beams in direct space. By comparing Fig. 3(b) with Fig. 3(a), one can see that higher index contrast enhances the high spatial frequency components which results in a stronger focalization and a narrower photonic jet. Nevertheless, whatever the index contrast, the microsphere produces high angular components in the scattered field when illuminated by an incident wave made of a single null-frequency component. This angular distribution provides to photonic jets the properties of a focused beam which will be helpful for the future investigations.

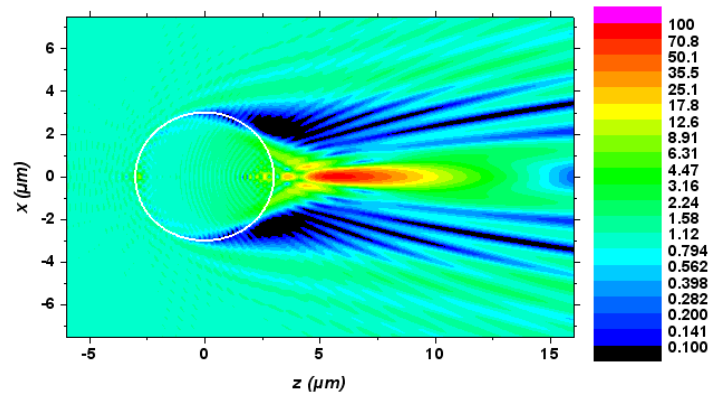
3. FROM PLANE WAVE TO THREE-DIMENSIONAL CONFINEMENT OF LIGHT

In low index contrast medium, the longitudinal dimension of photonic jets can be considered as a disadvantage because it does not provide a better confinement of light than a classical microscope objective with high numerical aperture. A simple manner to modify the features of the beam that emerges from the microsphere is to change the illumination beam. The numerical experiment has been undertaken recently to illuminate the microsphere with a highly focused Gaussian type beam and it has been demonstrated that the microsphere can confine the field at its surface in an intense volume smaller than $0.6 \times (\lambda/n)^3$ [24]. This phenomenon is due to the interplay of two contributions. A well-known focusing of the incident field by the microsphere provides the transversal confinement of the field. The longitudinal reduction is due to interferences between the scattered field and the high angular components of the excitation beam.

In this release, we study a full micrometric microscope objective made of compound dielectric microlenses in order to confine a plane wave in a three dimensional intense region of dimension on the order of the wavelength. We assume that the longitudinal confinement observed with a Gaussian beam illumination can be achieved with a photonic jet as incident beam. Owing to the study performed in the first section, which has demonstrated that photonic jets have high angular components, we propose to illuminate a second microsphere with a photonic jet. The aim is to reduce its longitudinal extent and make photonic jets suitable for applications requiring high transverse and longitudinal resolutions.

3.1 Reduction of the longitudinal extent of photonic jets

We consider a 6 μm -diameter latex sphere illuminated by a plane wave at $\lambda_v = 633$ nm. The figure 4(a) presents the electric field intensity maps of the photonic jet propagating in a water-based solution and illustrates, as discussed in the first part, its main features: a narrow lateral extent and a large longitudinal extent. The figure 4(b) shows the electric field intensity pattern when a 2 μm -diameter latex sphere is added in the photonic jet beam. The two spheres are touching and have the same optical axis. To simplify the study, the incident plane wave is circularly polarized to preserve the cylindrical symmetry. One can see from Fig. 7(b) that a single and bright spot of small dimensions in the three spatial directions is present at the surface of the smaller sphere.



(a)

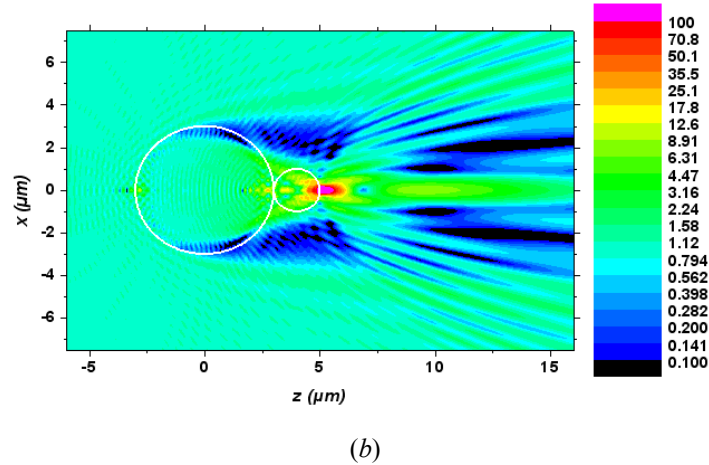


Fig. 4. Total electric field intensity map in logarithmic scale of (a) a 6 μm -diameter latex sphere illuminated by a plane wave at $\lambda_v = 633 \text{ nm}$ and (b) a 2 μm -diameter latex sphere is added in the photonic jet beam. The white circles represent the microspheres sections.

Table 1 compares the transverse and longitudinal waists (radii) of the two beams, defined at I_{max}/e^2 and denoted respectively w_{xy} and w_z . The longitudinal intensity distribution in figure 2(a) is not symmetric with respect to the I_{max} position and we define two longitudinal waists for the incident photonic jet beam, w_{z-} and w_{z+} , which are respectively the waists before and after the I_{max} position. The effective volume is then defined as $\pi^{3/2}w_{xy}^2(w_{z-}+w_{z+})/2$. The photonic jet is further confined by the second sphere both longitudinally and transversally. The effective volume behind the second sphere defined by $\pi^{3/2}w_{xy}^2w_z/2$ is reduced by more than one order of magnitude, and is approximately $(\lambda/n)^3$. Let us remark that the longitudinal waist is calculated outside the sphere. It is apparent that the longitudinal modification of the beam is more spectacular since the maximum intensity has both been enhanced and moved toward the sphere surface. It must be stressed that this strong confinement of light is obtained with a simple dielectric structure.

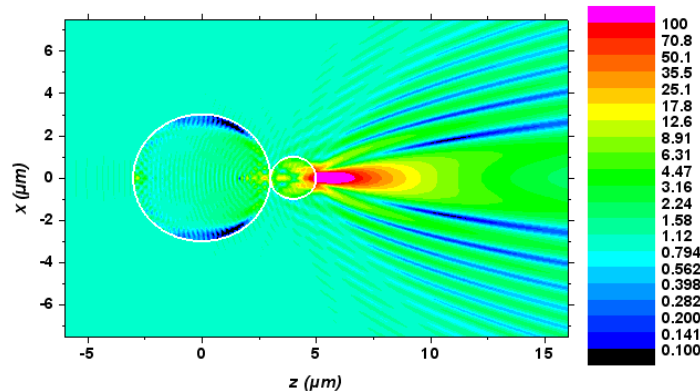


Fig. 5. Total electric field intensity map in logarithmic scale of the field scattered by the second sphere in the same condition than previously. The incident photonic jet has been removed from the field.

We employ our simulation method to calculate the incident and scattered field separately [24]. Figure 5 presents the map of the intensity of the field scattered by the second sphere. It shows an elongated region with high intensity in the shadow side of the sphere. This scattered field is very close to a classical “photonic nanojet” beam: it has both narrow lateral extent and large longitudinal extent. The coherent sum of the field scattered by the bigger sphere plus the scattered field by the second one is able to reach the strong confinement in the three directions (Fig. 4(b)).

	Photonic jet	Photonic jet + second microsphere
Transverse waist w_{xy}	370 nm	225 nm
Longitudinal waist w_z	$w_{z^-} = 1400$ nm $w_{z^+} = 4590$ nm	795 nm
Maximum intensity	87.5	420
Effective volume V	$2.3 \mu\text{m}^3$ $\approx 21 (\lambda/n)^3$	$0.11 \mu\text{m}^3$ $\approx 1.05 (\lambda/n)^3$

Table 1. Summary of the characteristics widths at I_{max}/e^2 corresponding to the intensity maps displayed in Figs. 7(a) and 1(b). The volume is derived for the incident photonic jet as $V = \pi^{3/2} w_{xy}^2 (w_z + w_{z^+})/2$, and for the field focused by the microsphere as $V = \pi^{3/2} w_{xy}^2 w_z/2$ (let us recall that only the beam exiting the microsphere is considered here).

3.2 Discussions

We have demonstrated that the longitudinal dimension of photonic jets could be strongly reduced using a microsphere placed in the photonic jet beam. An incident plane wave can be strongly confined in a volume on the order of $(\lambda/n)^3$ using a simple configuration. The confinement of photonic jets is based on the same principles that the confinement achieved when the microsphere is illuminated by a highly focused Gaussian beam [24]. The classical focusing by a microsphere can only provide a transversal confinement. The reduction of the longitudinal dimension is obtained from interferences between the field scattered by the microsphere and the high angular components of the incident beam.

The position of the microsphere is a critical point to achieve the confinement. It has been shown that a minimum exists and occurs when the center of the microsphere is placed a few micrometers before the incident focusing position. In the present case, we have considered that the two spheres are touching. Then, the diameter of the second sphere sets the distance to the focus of the incident photonic jet. To enable the same longitudinal reduction effect, the photonic jet used as incident beam must be separate from the sphere surface in order to set the second microsphere in a proper position. This effect can be achieved only when the index contrast between the microspheres and the host medium is low.

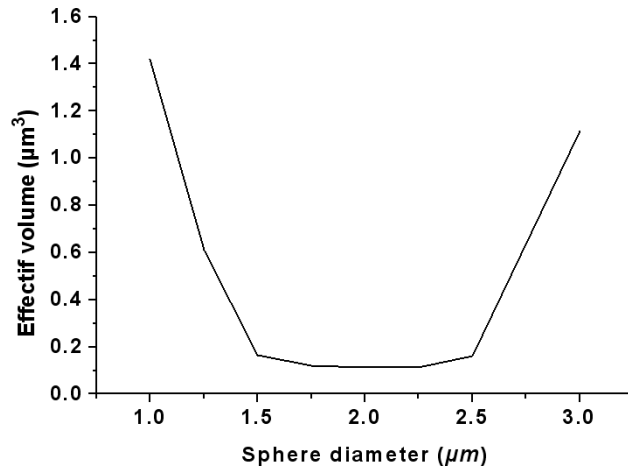


Fig. 6. Effective volume as a function of the second sphere diameter. The incident photonic jet is obtained using the 6 μm diameter latex microsphere.

The figure 6 displays the effective volume of the hot spot obtained in the presence of the second sphere with respect to its diameter. This plot shows a minimum for a 2 μm-diameter sphere. The intensity map of the two extreme configurations is displayed in figure 7 for the smaller sphere of diameter (a) 1 μm and (b) 3 μm. When the sphere is too small (Fig. 7(a)), most of the energy is passing aside the sphere so that the photonic jet is almost not modified. When the

sphere exceeds a critical size as illustrated in Figure 7(b), the whole beam penetrates the sphere, the maximum intensity occurs inside the sphere which is of minor interest. In addition, an intense field still exists at the exit surface of the sphere but it is no more confined. The distribution pattern shows a transversal confinement of the field but no destructive interferences that could have enabled the longitudinal reduction. The effective volume is ten times larger than in the optimal case.

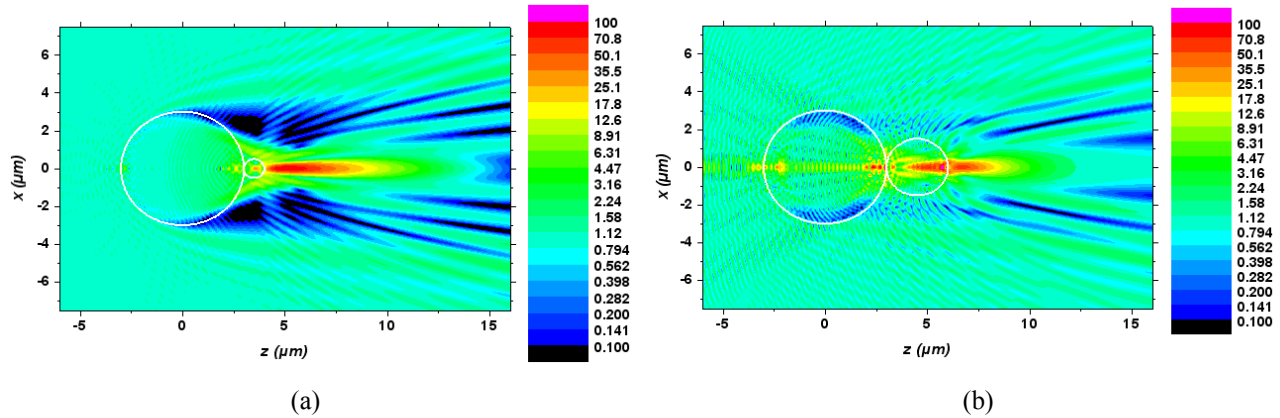


Fig. 7. Total electric field intensity map in logarithmic scale of a 6 μm -diameter latex sphere illuminated by a plane wave at $\lambda_v = 633 \text{ nm}$ (a) a 1 μm -diameter latex sphere is added in the photonic jet beam and (b) a 3 μm -diameter latex sphere is added in the photonic jet beam. The white circles represent the microsphere sections.

It could be stressed that the fabrication of this compound set of two dielectric microspheres is not trivial and should require technically challenging processes. However, this numerical study permits to better understand the longitudinal confinement of light observed when the microsphere is illuminated by a highly focused beam. Moreover, it highlights that microscope objectives of micrometric sizes can be designed in principle. For instance, the respective index contrasts of the two microlenses could be tailored to compensate chromatic aberrations analogously to the classical achromatic doublets.

4. CONCLUSION

The reduction of the longitudinal dimension of photonic nanojets has been demonstrated. It is based on the ability of microspheres to confine a highly focused beam along the three spatial directions. We demonstrated that an optical plane wave can be confined in a volume of order $(\lambda/n)^3$ by a compound set of dielectric microspheres. This could be particularly helpful in applications where high resolution is required with low index contrasts.

REFERENCES

- [1] J.-C. Weeber, A. Bouhelier, G. Colas des Francs, L. Markey, and A. Dereux, "Submicrometer In-Plane Integrated Surface Plasmon Cavities," *Nano Lett.* **7**, 1352-1359 (2007).
- [2] H. Rigneault, J. Capoulade, J. Dintinger, J. Wenger, N. Bonod, E. Popov, T. W. Ebbesen, P.F. Lenne, "Enhancement of single-molecule fluorescence detection in subwavelength apertures," *Phys. Rev. Lett.* **95**, 117401 (2005).
- [3] P. Anger, P. Bharadwaj and L. Novotny, "Enhancement and Quenching of Single-Molecule Fluorescence," *Phys. Rev. Lett.* **96**, 113002 (2006).
- [4] S. Nie, S. R. Emory, "Probing single molecules and single nanoparticles by surface-enhanced Raman scattering," *Science* **275**, 1102 (1997).
- [5] S. Noda, "Seeking the ultimate nanolaser," *Science* **314**, 260-261 (2006).
- [6] A. Sentenac and P. C. Chaumet, "Subdiffraction Light Focusing on a Grating Substrate," *Phys. Rev. Lett.* **101**, 013901 (2008).

- [7] D. C. Marinica, A. G. Borisov, S. V. Shabanov, "Bound states in the continuum in photonics," *Phys. Rev. Lett.* **100**, 183902 (2008).
- [8] Z. Chen, A. Taflove, V. Backman, "Photonic nanojet enhancement of backscattering of light by nanoparticles: A potential novel visible-light ultramicroscopy technique," *Opt. Express* **12**, 1214 - 1220 (2004).
- [9] X. Li, Z. Chen, A. Taflove, V. Backman, "Optical analysis of nanoparticles via enhanced backscattering facilitated by 3-D photonic nanojets," *Opt. Express* **13**, 526 - 533 (2005).
- [10] S. Lecler, Y. Takakura, and P. Meyrueis, "Properties of a 3D photonic jet," *Opt. Lett.* **30**, 2641-2643 (2005).
- [11] A. V. Itagi and W. A. Challener, "Optics of photonic nanojets," *J. Opt. Soc. Am. A* **22**, 2847-2858 (2005).
- [12] J. Kofler, N. Arnold, "Axially symmetric focusing as a cuspid diffraction catastrophe: scalar and vector cases and comparison with the theory of Mie," *Phys. Rev. B.* **73**, 235401 (2006).
- [13] P. Ferrand, J. Wenger, A. Devilez, M. Pianta, B. Stout, N. Bonod, E. Popov, and H. Rigneault, "Direct imaging of photonic nanojets," *Opt. Express* **16**, 6930-6940 (2008).
- [14] A. Devilez, B. Stout, N. Bonod, E. Popov, "Spectral analysis of three-dimensional photonic jets," *Opt. Express* **16**, 14200 - 14212 (2008).
- [15] M. Mosbacher, H.-J. Münzer, J. Zimmermann, J. Solis, J. Boneberg, P. Leiderer, "Optical field enhancement effects in laser-assisted particle removal," *Appl. Phys. A: Mater. Sci. Process.* **72**, 41-44 (2001).
- [16] B. S. Luk'yanchuk, N. Arnold, S. M. Huang, Z. B. Wang, and M. H. Hong, "Three-dimensional effects in dry laser cleaning," *Appl. Phys. A: Mater. Sci. Process.* **77**, 209-215 (2003).
- [17] K. Piglmayer, R. Denk, and D. Bäuerle, "Laser-induced surface patterning by means of microspheres," *Appl. Phys. Lett.* **80**, 4693-4695 (2002).
- [18] E. McLeod, C. B. Arnold, "Subwavelength direct-write nanopatterning using optically trapped microspheres," *Nature nanotechnology* **3**, 413 - 417 (2008).
- [19] A. Pereira, D. Grojo, M. Chaker, P. Delaporte, D. Guay, M. Sentis, "Laser-fabricated porous alumina membranes for the preparation of metal nanodot arrays," *Small* **4**, 572-576 (2008)
- [20] K. J. Yi, H. Wang, Y. F. Lu, Z. Y. Yang, "Enhanced Raman scattering by self-assembled silica spherical microparticles," *J. Appl. Phys.* **101**, 063528 (2007).
- [21] J. Kasim, Y. Ting, Y. Y. Meng, L. J. Ping, A. See, L. L. Jong, S. Z. Xiang, "Near-field Raman imaging using optically trapped dielectric microsphere," *Opt. Express* **16**, 7976 - 7984 (2008).
- [22] S.-C. Kong, A. Sahakian, A. Taflove, V. Backman, "Photonic nanojet-enabled optical data storage," *Opt. Express* **16**, 13713 - 13719 (2008).
- [23] D. Gérard, J. Wenger, A. Devilez, D. Gachet, B. Stout, N. Bonod, E. Popov, H. Rigneault, "Strong electromagnetic confinement near dielectric microspheres to enhance single-molecule fluorescence," *Opt. Express* **16**, 15297 - 15303 (2008).
- [24] A. Devilez, N. Bonod, J. Wenger, D. Gérard, B. Stout, H. Rigneault, E. Popov, "Three-dimensional subwavelength confinement of light using dielectric microspheres," *Opt. Express* **17**, 2089 - 2094 (2009).
- [25] B. Stout, M. Neviere, E. Popov, "Light diffraction by three-dimensional object: differential theory," *J. Opt. Soc. Am. A* **22**, 2385 - 2404 (2005).
- [26] L. W. Davis, "Theory of electromagnetic beams," *Phys. Rev. A* **19**, 1177 - 1179 (1978).
- [27] B. Stout, J.-C. Auger, J. Lafait, "A transfer matrix approach to local field calculations in multiple-scattering problems," *J. Mod. Opt.* **49**, 2129 - 2152 (2002).